On the Contribution of Roughness Effects to the Scaling of Ship Resistance

L.Eça*, A.R.Starke†, M.Kerkvliet† and H.C.Raven†

*MARIN Academy, Instituto Superior Técnico (IST), ULisbon
Av. Rovisco Pais 1, 1049-001 Lisboa, Portugal
e-mail: luis.eca@tecnico.ulisboa.pt

† Maritime Research Institute Netherlands (MARIN)
Haagsteeg 2, 6708 PM Wageningen, The Netherlands
e-mail: B.Starke@marin.nl, M.Kerkvliet@marin.nl, H.C.Raven@marin.nl

* Corresponding author: L.Eça

ABSTRACT

Roughness effects are one of the main challenges of the prediction of ship resistance using traditional model tests and extrapolation procedures. Computational Fluid Dynamics (CFD) can play an important role in the improvement of empirical correlations. Nowadays, most CFD RANS solvers use an equivalent sand-grain roughness height to model roughness effects. Therefore, the simulation of roughness effects includes two main challenges: estimate the equivalent sand-grain roughness height that corresponds to a given average roughness height typically used to characterize the roughness of ships; include sand-grain roughness effects in the most accurate RANS turbulence models for the simulation of ship flows, as for example the $k-\omega$ SST eddy-viscosity model.
In this work, the flows around different geometries (flat plate, submarine and two ships) at full scale Reynolds numbers (10^8 to 10^9) are simulated with RANS solvers using the $k-\omega$ SST eddy-viscosity model. Roughness effects are included in the k and ω boundary conditions for values of the sand-grain roughness height covering hydraulically smooth and fully-rough surfaces. It is shown that with the proper scaling, the increase of the friction resistance coefficient with the sand-grain roughness height is equivalent for the four geometries tested. Conversion of average roughness height to sand-grain roughness is assessed by comparing CFD results with Bowden and Davison and Townsin *et al.* empirical correlations. Results of the simulations show the best agreement with the Townsin *et al.* correlation with a small variation of the ratio between average roughness and sand-grain roughness heights.
Keywords: Sand-grain Roughness; CFD; Scale effects; RANS;

1 INTRODUCTION

One of the key parameters for the design and operation of a ship is its resistance coefficient. Model testing has been traditionally used to address this problem. However, this leads to a well known scaling problem due to the mismatch between the full scale and model scale Reynolds numbers. From the several problems introduced by this scaling effect, surface roughness is one of the most troublesome to address. In fact, model testing is normally performed with hydraulically smooth surfaces whereas most full scale ships exhibit rough surfaces.
In the ITTC (2008) scaling procedure, roughness effects are included in the so-called correlation allowance, ΔC_F, which is determined as a function of the Average Hull Roughness (AHR) divided by the ship length L_{PP} (Bowden B.S. and Davison N.J. 1974). Other proposals available in the open literature are also listed in ITTC (2008) for roughness effects in ship resistance as for example those of Townsin *et al.* (1984) and Himeno that also use AHR/L_{PP} to characterize the ship roughness. These

roughness correlations have been tested in many experimental studies as for example in the study presented by Yeginbayeva and Atlar (2018).
The ability to characterize surface roughness using a single parameter as AHR is questioned by Townsin et. al (1984) and Anderson *et al.* (2020). However, this topic is out of the scope of the present paper. Nonetheless, we recall the procedure that leads to the determination of AHR. The standard measure of hull roughness is $Rt(50)$ which is a measure of the maximum peak-to-valley height over 50 mm lengths of the hull surface. Several values of $Rt(50)$ are determined at a particular location on the hull and these are combined to give a Mean Hull Roughness (MHR) at that location. The Average Hull Roughness AHR) is an attempt to combine the individual MHR values into a single parameter. Typically the MHR is determined at various positions on the hull and then combined to give the AHR for the entire vessel.
In computational fluid dynamics (CFD), roughness is typically modelled using an equivalent sand-grain roughness height h_{sg}. Therefore, the first challenge for simulating roughness effects in ship flows is the relation between AHR and h_{sg}, which is not a trivial problem. Schultz (2007) indicates that h_{sg} should be approximately five times smaller than AHR for ships with an antifouling coating. However, as discussed by Anderson *et al.* (2020) this relation may be case dependent.
The second challenge of CFD is to incorporate sand-grain roughness effects in the mathematical model. For the Reynolds-averaged Navier-Stokes (RANS) equations, the typical approach is to incorporate roughness effects using wall functions or changing the wall boundary conditions of the dependent variables of the turbulence model, see for example (Eça and Hoekstra 2011). Aupoix (2014) presents several approaches for the inclusion of sand-grain roughness effects in the $k-\omega$ shear-stress transport (SST) two-equation eddy-viscosity model (Menter 1984) without the use of wall functions. In the approach proposed by Hellsten and Laine (1998) roughness affects the ω wall boundary condition and the limiter of the eddy-viscosity. Knopp *et al.* (2009) and two new proposals use the k and ω wall boundary conditions to introduce roughness effects. Two of these approaches (Knopp *et al.* 2009 and Hellsten and Laine 1998) have been tested in ship flows (Eça, Hoekstra and Raven 2010) and its results compared with the empirical correlations presented in the ITTC (2008) report. In that study, the relation between h_{sg} and AHR suggested by Schultz (2007) is adopted.
In the present study, the RANS equations using the $k-\omega$ SST two-equation eddy-viscosity model (Menter 1994) are solved for four different incompressible flows of a single-phase Newtonian fluid including rough surfaces using the PARNASSOS (Hoekstra and Eça 1998) and ReFRESCO (2021) flow solvers. In the first part of the study, the simple flow over a flat plate of length L is simulated for values of h_{sg} leading to surfaces ranging from the hydraulically smooth to the fully-rough regime. The techniques discussed by Aupoix (2014) except the Wilcox (1988) proposal that is not suitable for the SST version of the $k-\omega$ model are evaluated. The skin friction coefficients are compared with empirical correlations available for the fully-rough regime (Mills and Xu Hang, 1983) and the constants of the log-law region are determined as a function of Re_x and h_{sg}/L.
In the second part of the study, the Hellsten and Laine (1998) approach is applied to the simulation of the flow around three different geometries at full scale Reynolds numbers: the generic submarine BB2, for which over the last years a variety of collaborative studies were conducted (Carrica *et al.* 2016 and Toxopeus *et al.* 2019); the KVLCC2 tanker that has been a test case of the numerical ship hydrodynamics workshops of 2000 and 2010 (Larsson *et al.* 2000 and 2010); the so-called Japan Bulk Carrier (JBC) that has been used in the 2015 workshop on numerical ship hydrodynamics (Hino *et al.* 2016). As for the flat plate case, several values of h_{sg}/L_{PP} are tested for each test case and Reynolds number. The objective of this part of the study is twofold:

1. Investigate alternative ways to describe the increase of friction resistance with the roughness height that allow to collapse the data obtained for all geometries to a single line;

2. Fit the numerical results to the empirical correlations based on AHR/L_{PP} to estimate the ratio between h_{sg} and AHR.

The remaining of this paper is organized in the following way: section 2 presents the mathematical model and the techniques to handle roughness effects; test cases, boundary conditions and numerical

details are given in section 3; section 4 presents and discusses the results of the simulations and the conclusions of this study are summarized in section 5.

2 MATHEMATICAL MODEL

Time-averaging is applied to the flow properties and to mass conservation and momentum balance to obtain the continuity and Reynolds-Averaged (RANS) equations, which using an eddy-viscosity model can be written as

$$\frac{\partial V_i}{\partial x_i} = 0 \ , \tag{1}$$

$$\frac{\partial V_j V_i}{\partial x_j} = -\frac{1}{\rho}\frac{\partial P}{\partial x_i} + \frac{\partial}{\partial x_j}\left[(\nu + \nu_t)\left(\frac{\partial V_i}{\partial x_j} + \frac{\partial V_j}{\partial x_i}\right)\right] \ , \tag{2}$$

where $x_i \equiv (x_1, x_2, x_3)$ are the coordinates of a Cartesian coordinate system, V_i are the components of the mean velocity vector, P is the average pressure[1], ν is the kinematic viscosity of the fluid and ν_t is the eddy-viscosity that is obtained with the $k-\omega$ SST two-equation, eddy-viscosity model (Menter 2003).

$$\nu_t = \frac{a_1 k}{\max\left(a_1\omega, F_2 S\right)} \ . \tag{3}$$

$a_1 = 0.31$, $S = \sqrt{2S_{ij}S_{ij}}$ where S_{ij} are the components of the mean strain rate tensor and F_2 is a function defined by

$$F_2 = \tanh\left[\left(\max\left(2\frac{\sqrt{k}}{\beta^*\omega d}, \frac{500\nu}{\omega d^2}\right)\right)^2\right] \ ,$$

where $\beta^* = 0.09$ and d is the distance to the wall.
The k transport equation is given by

$$V_i\frac{\partial k}{\partial x_i} = P_k + \frac{\partial}{\partial x_i}\left((\nu + \sigma_k\nu_t)\frac{\partial k}{\partial x_i}\right) - \beta^*\omega k \ , \tag{4}$$

where $\sigma_k = 1 - 0.15F_1$.
The production term is limited proportionally to the dissipation term,

$$P_k = \min\left(\nu_t S, 15\beta^*\omega k\right) \ .$$

F_1 is a blending function, (Menter 2003), given by

$$F_1 = \tanh\left(arg^4\right) \ , \tag{5}$$

with

$$arg = \min\left(\max\left(\frac{\sqrt{k}}{\beta^*\omega d}, \frac{500\nu}{\omega d^2}\right), \frac{4\sigma_{\omega 2}k}{CD_{k\omega}d^2}\right)$$

and

$$CD_{k\omega} = \max\left(\frac{2\sigma_{\omega 2}}{\omega}\frac{\partial k}{\partial x_i}\frac{\partial \omega}{\partial x_i}, 10^{-10}\right)$$

with $\sigma_{\omega 2} = 0.856$.
The ω transport equation is

$$V_i\frac{\partial \omega}{\partial x_i} = \frac{\gamma}{\nu_t}P_k + \frac{\partial}{\partial x_i}\left((\nu + \sigma_\omega\nu_t)\frac{\partial \omega}{\partial x_i}\right) - \beta\omega^2 + 2\left(1 - F_1\right)\frac{\sigma_{\omega 2}}{\omega}\frac{\partial k}{\partial x_i}\frac{\partial \omega}{\partial x_i} \ , \tag{6}$$

where $\gamma = 0.44 + 0.1156F_1$, $\sigma_\omega = 0.856 - 0.356F_1$ and $\beta = 0.0828 - 0.0078F_1$.

2.1 Roughness effects

Four alternative techniques are tested that do not apply wall functions and use the wall boundary conditions of the turbulence quantities to introduce the roughness effects.

[1] P is the relative pressure with the hydrostatic pressure as the reference and it contains the $2/3k$ contribution of the normal Reynolds stresses, where k is the turbulence kinetic energy.

2.1.1 Hellsten and Laine proposal, HL1998

In the Hellsten and Laine (1998), k at the wall is equal to zero as for smooth surfaces and the ω wall boundary condition is identical to that proposed in Wilcox (1988) and updated in Wilcox (2006)

$$\omega_w = \frac{u_\tau^2 S_R}{\nu} \ , \tag{7}$$

where u_τ is the friction velocity obtained from the shear-stress at the wall τ_w ($u_\tau = \sqrt{\tau_w/\rho}$) and

$$S_R = \begin{cases} \left(\dfrac{200}{h_{sg}^+}\right)^2 & \Leftarrow \quad h_{sg}^+ \leq 5 \\ \dfrac{100}{h_{sg}^+} + \left[\left(\dfrac{200}{h_{sg}^+}\right)^2 - \dfrac{100}{h_{sg}^+}\right] \exp\left(5 - h_{sg}^+\right) & \Leftarrow \quad h_{sg}^+ > 5 \end{cases} \tag{8}$$

h_{sg}^+ is sand-grain roughness height in wall coordinates

$$h_{sg}^+ = \frac{u_\tau h_{sg}}{\nu} \ . \tag{9}$$

This definition of ω_w affects the limiter used in the calculation of ν_t of the SST $k-\omega$ model and so equation (3) was modified by Hellsten and Laine (1998) to

$$\nu_t = \frac{a_1 k}{\max\left(a_1\omega, F_2 F_3 S\right)} \ , \tag{10}$$

where

$$F_3 = 1 - \tanh\left[\left(\frac{150\nu}{\omega d^2}\right)^4\right] \ . \tag{11}$$

2.1.2 Knopp *et al.* proposal, K2009

The technique proposed by Knopp *et al.* (2009) is based on the wall values of k and ω.

$$k_w = \min\left(1, \frac{h_{sg}^+}{90}\right) \frac{u_\tau^2}{\sqrt{\beta^*}} \ , \tag{12}$$

$$\omega_w = \frac{u_\tau}{\sqrt{\beta^*}\kappa d_o} \tag{13}$$

with $\kappa = 0.41$ and

$$d_o = 0.03 h_{sg} \min\left[1, \left(\frac{h_{sg}^+}{30}\right)^{2/3}\right] \min\left[1, \left(\frac{h_{sg}^+}{45}\right)^{1/4}\right] \min\left[1, \left(\frac{h_{sg}^+}{60}\right)^{1/4}\right] \ . \tag{14}$$

2.1.3 Aupoix proposal based on the Nikuradse correlation, AN2014

Aupoix (2014) derives alternative k and ω wall boundary conditions based on the Nikuradse correlation.

$$k_w = \max\left(0, \frac{u_\tau^2}{\sqrt{\beta^*}} \tanh\left[\left(\frac{\ln\left(\dfrac{h_{sg}^+}{30}\right)}{\ln(8)} + 0.5\left[1 - \tanh\left(\frac{h_{sg}^+}{100}\right)\right]\right) \tanh\left(\frac{h_{sg}^+}{75}\right)\right]\right) \ , \tag{15}$$

$$\omega_w = \frac{u_\tau^2}{\nu}\left[\frac{400000}{(h_{sg}^+)^4}\left(\tanh\left(\frac{10000}{3(h_{sg}^+)^3}\right)\right)^{-1} + \frac{70}{h_{sg}^+}\left(1 - \exp\left(-\frac{h_{sg}^+}{300}\right)\right)\right] \ . \tag{16}$$

This alternative is aimed at roughness sizes in the intermediate regime.

2.1.4 Aupoix proposal based on the Colebrook results, AC2014

Aupoix (2014) also presents an alternative for roughness sizes in the fully-rough regime, which is based on Grigson's representation of Colebrook's results.

$$k_w = \max\left(0, \frac{u_\tau^2}{\sqrt{\beta^*}}\tanh\left[\left(\frac{\ln\left(\frac{h_{sg}^+}{30}\right)}{\ln(10)} + 1 - \tanh\left(\frac{h_{sg}^+}{125}\right)\right)\tanh\left(\frac{h_{sg}^+}{125}\right)\right]\right) , \tag{17}$$

$$\omega_w = \frac{u_\tau^2}{\nu}\left[\frac{300}{(h_{sg}^+)^2}\left(\tanh\left(\frac{15}{4h_{sg}^+}\right)\right)^{-1} + \frac{191}{h_{sg}^+}\left(1 - \exp\left(-\frac{h_{sg}^+}{250}\right)\right)\right] . \tag{18}$$

3 TEST CASES AND NUMERICAL DETAILS

3.1 Geometries and Flow Conditions

Four different geometries have been selected for this study: preliminary results are obtained for a flat plate; a generic submarine and two ships are used to assess the estimation of roughness effects in practical applications.

3.1.1 Flat plate

For the simulation of the statistically steady, two-dimensional flow of an incompressible fluid over a flat plate, the computational domain is a rectangle with the incoming flow V_∞ and the plate of length L aligned with the horizontal direction x. The leading edge of the plate is located at the origin of the (x, y) Cartesian coordinate system. The length of domain is $1.5L$ with the inlet located at $-0.25L$ and the outlet at $0.25L$. Two Reynolds numbers Re based on the undisturbed incoming velocity V_∞, length of the plate L ($Re = V_\infty L/\nu$) are tested: $Re = 10^7$ and $Re = 10^9$. The range of values of h_{sg}/L tested lead to

$$0 \leq \frac{V_\infty h_{sg}}{\nu} \leq 4400 .$$

The computational domain illustrated in figure 1 has been tested in several previous studies as for example (Eça and Hoekstra 2008, Eça *et al.* 2018).

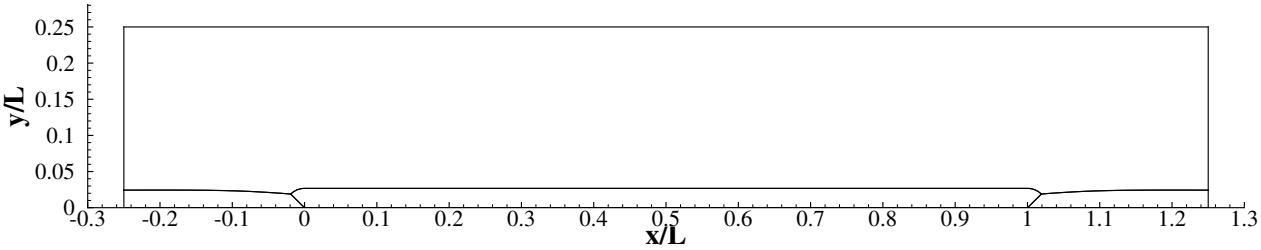

Figure 1. Illustration of the domain for the calculation of the flow over a flat plate at a Reynolds number of 10^7.

3.1.2 BB2 generic submarine

The BB2 submarine is displayed in figure 2 and it has a length $L_{\text{oa}} = 70.2$m. The computational domain includes only half the submarine and it has a parallelepipedic shape with a longitudinal length (aligned with the incoming flow) of $7.2L_{\text{oa}}$ in streamwise direction with $2.5L_{\text{oa}}$ in front of the bow, a total height of $6L_{\text{oa}}$ with the submarine in the middle and a width of $3L_{\text{oa}}$. The Reynolds

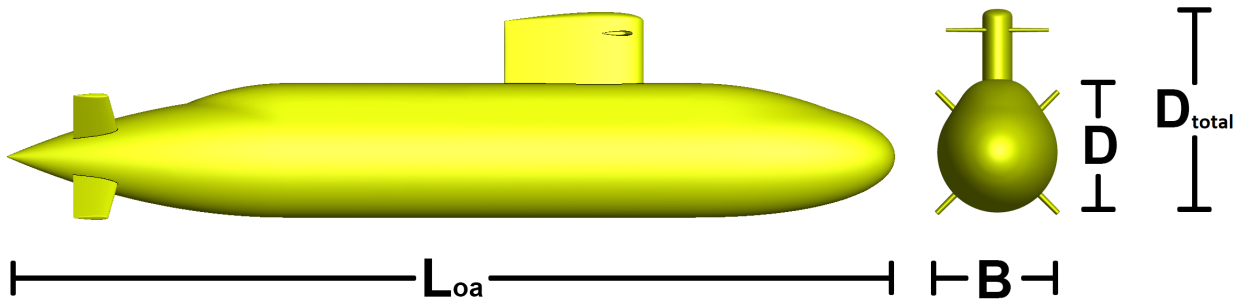

Figure 2. BB2 generic submarine geometry and main dimensions.

number based on V_∞ and L_{oa} is $Re = 3.25 \times 10^8$. The range of sand-grain roughness heights is between 0 and 2685 μm that leads to

$$0 \leq \frac{V_\infty h_{sg}}{\nu} \leq 12400 \, .$$

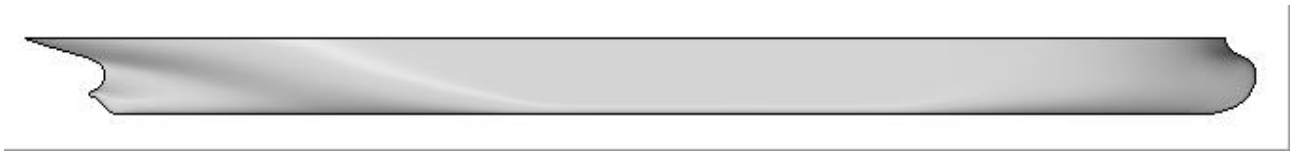

Figure 3. KVLCC2 geometry.

3.1.3 KVLCC2 tanker

The KVLCC2 tanker has a length of $L_{PP} = 320$m and its geometry is illustrated in figure 3. The computational domain for the KVLCC2 tanker covers also half the ship and it has a parallelepipedic shape with incoming flow aligned with the longitudinal direction. The inlet plane is located L$_P P$ upstream of the bow and the outlet plane $2L_{PP}$ downstream of the stern. The width of the domain is L_{PP} and the height is $1.065L_{PP}$. This domain has been used in the study presented by Pereira *et al.* (2019). The Reynolds number based on the incoming flow velocity V_∞ and L_{PP} is $Re = 2 \times 10^9$. Sand-grain roughness height is varied between 0 and 1536μm that leads to

$$0 \leq \frac{V_\infty h_{sg}}{\nu} \leq 9600 \, .$$

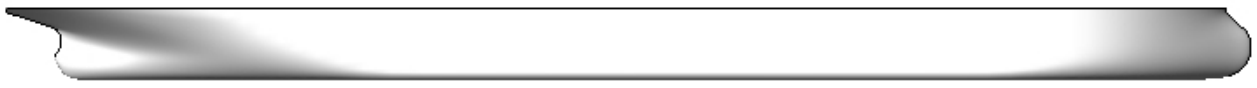

Figure 4. Japan Bulk Carrier (JBC) geometry.

3.1.4 Japan Bulk Carrier

The Japan Bulk Carrier geometry is illustrated in figure 4 and it has a length $L_{PP} = 280$m. As for the previous cases, the computational domain includes only half the ship and it has a parallelepipedic shape with the longitudinal direction aligned with the incoming flow. The inlet plane is located $0.5L_{PP}$ upstream of the bow and the outlet $1.5L_{PP}$ aft of the transom. The width and height of the domain

are equal to L_{PP}. Three Reynolds numbers based on V_∞ are tested: $Re = 1.33 \times 10^9$, $Re = 1.84 \times 10^9$ and $Re = 2.34 \times 10^9$. For each Re, h_{sg} is varied between 0 and 800μm, which leads to a largest value of $V_\infty h_{sg}/\nu \simeq 5260$.

3.2 Boundary Conditions

There are several boundary conditions that are common to the four geometries. At the inlet of the domain, the velocity components are specified from the incoming uniform flow and the pressure is extrapolated from the interior for all cases, except the JBC where a potential-flow solution provides the inlet velocity profiles. Turbulence quantities k and ω are also specified at the inlet boundary. Table 1 summarizes the values of turbulence intensity I and ν_t used to derive the inlet values of k and ω.

Table 1. Inlet values of turbulence intensity I and eddy-viscosity ν_t for each test case.

	Flat Plate		BB2	KVLCC2	JBC
Re	10^7	10^9	3.25×10^8	2×10^9	$1.33, 1.84, 2.34 \times 10^9$
I	0.01	0.01	0.05	0.01	$\sqrt{\frac{0.1}{1.5Re}}$
ν_t/ν	0.1	10.	1.	10.	10.

Symmetry conditions are applied at several boundaries: symmetry planes upstream and downstream of the flat plate; symmetry planes of the BB2 generic submarine, KVLCC2 and JBC ships; still water plane (top boundaries) of the double body calculations for the KVLCC2 and JBC.
At the surface of all the bodies the no-slip condition is applied without the use of wall functions. Pressure derivative in the direction normal to the wall is set equal to zero and turbulence quantities are used to include roughness effects as presented in section 2.1. For the smooth surfaces ω is specified at the first interior node/cell centre away from the wall (Eça and Hoekstra 2004).

3.2.1 Flat plate

At the top boundary of the domain, the pressure is imposed and the normal derivatives of all remaining variables is set equal to zero. At the outlet boundary, the streamwise derivatives of all dependent variables is set equal to zero.

3.2.2 BB2 generic submarine

For the BB2, at the top, bottom and side boundaries the pressure is imposed and normal derivatives are set equal to zero for all remaining variables.

3.2.3 KVLCC2 tanker

Free slip conditions are applied at the lateral and bottom boundaries of the domain. At the outlet plane, the pressure is imposed, whereas the streamwise derivatives of all remaining variables are set equal to zero.

3.2.4 Japan Bulk Carrier

At the external boundary the pressure and two tangential velocity components have been taken from a potential-flow solution and the normal velocity component at that boundary then follows from the continuity equation. At the outlet plane the streamwise derivatives of all variables are set equal to zero.

3.3 Numerical Details

3.3.1 Flow solvers

The calculations of the flows over the flat plate and around the BB2 generic submarine and the KVLCC2 tanker have been performed with ReFRESCO (2021), which is based on a finite-volume discretization with collocated variables. Second-order schemes are used for the discretization of all terms of the transport equations with the exception of the KLVCC2 tanker simulations that have been performed with first-order upwind in the convective terms of the k and ω transport equations. ReFRESCO solution procedure is based on the SIMPLE algorithm and a segregated approach is used to solve the several transport equations.
On the other hand, the finite-difference based solver PARNASSOS (Hoekstra and Eça 1998) is used in the simulations of the flow around the JBC. PARNASSOS uses a fully-coupled approach with the continuity equation solved without any modification. Convective terms of the momentum equations are approximated with third-order upwind schemes, whereas first-order upwind is used for the convective terms of the k and ω transport equations. Remaining terms are all approximated with second-order schemes.

3.3.2 Grids

Multiblock-structured grids have been used for all test cases. For the flat plate at $Re = 10^7$, a formal grid refinement study has been performed that indicated that the grid convergence properties are not significantly affected by the surface roughness. Therefore, in the present study we have favoured increasing the number of values of h_{sg} tested instead of performing formal grid refinement studies for all test cases. Nonetheless, we can point out the numerical uncertainties estimated for the friction resistance coefficient and skin friction coefficient of the flat plate case are less than 1%.
The grids of all test cases exhibit a largest near-wall cell height in wall coordinates smaller than 1 ($y^+ < 1$). The number of cell faces on the surface of the four geometries tested is 1,024 for the flat plate 102,114 for the BB2, 46,800 for the KVLCC2 and approximately 17,000 for the JBC. Figure 5 presents views of details of the grids used in this study.

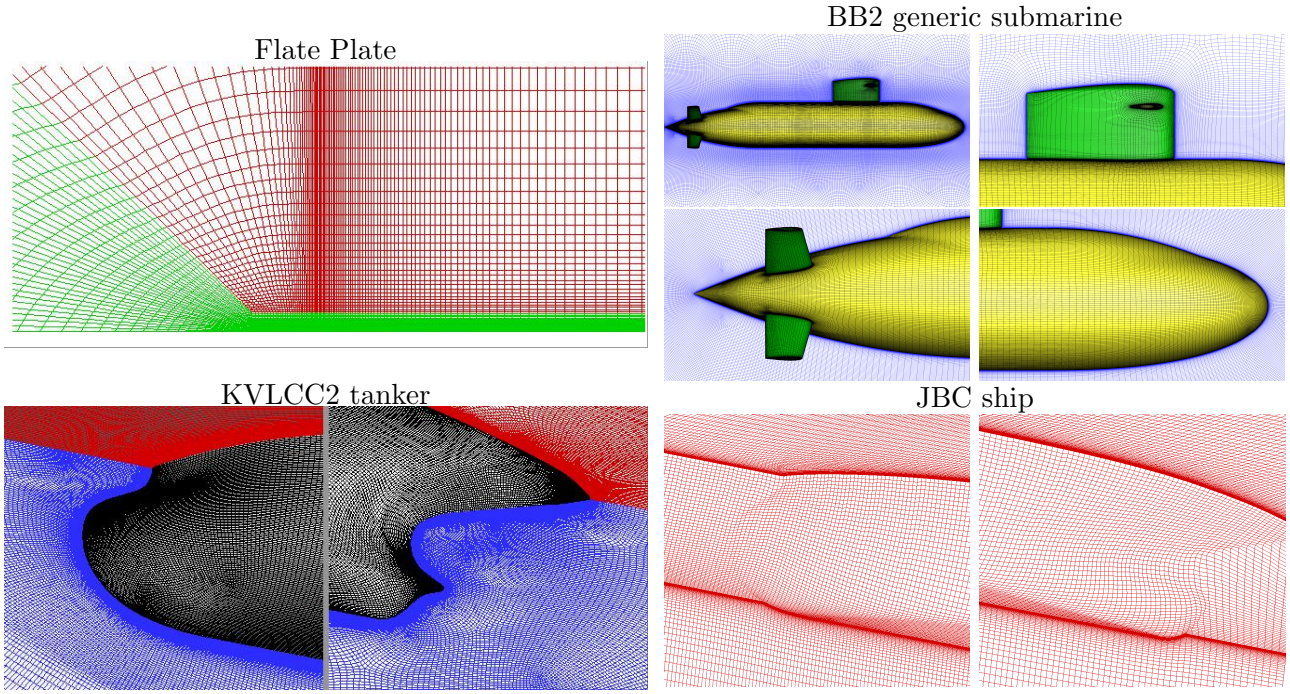

Figure 5. Illustration of the grids used for the four selected geometries.

3.3.3 Iterative Convergence

Both flow solvers monitor iterative convergence using normalized (dimensionless) residuals and differences between successive iterations. Convergence criteria is not identical for the all the simulations. All simulations were performed with double precision (14 digits), but only the flat plate simulations were iteratively converged almost to machine accuracy. Nonetheless, for the three-dimensional simulations iterative convergence criteria was sufficient to guarantee a negligible effect in friction force coefficients.

4 RESULTS

The calculations performed for the four test cases have different goals. The flow over a flat plate at $Re = 10^7$ and $Re = 10^9$ is used to assess the four alternative formulations to represent roughness effects. On the other hand, the objectives of the simulations of the flows around the BB2 generic submarine, KVLCC2 and JBC ships are to investigate dimensionless representations of roughness effects on the friction resistance coefficient and to assess the conversion of AHR to h_{sg}.
For the sake of simplicity, we will refer to the four alternative techniques to simulate roughness effects as HL1998 for Hellsten and Laine (1998), K2009 for Knopp *et al.* (2009), AN2014 and AC2014 for the Aupoix (2014) approaches based on the Nikuradse (AN2014) and Colebrook (AC2014) correlations.

4.1 Alternative Formulations of Roughness Effects

4.1.1 Reference data

According to Churchill S.W. (1993), a good fit to the skin friction coefficient of the flow over a flat plate measured by Pimenta *et al.* (1975) is presented by Mills and Hang (1973):

$$C_f = \left(a_1 + a_2 \ln\left(\frac{x}{h_{sg}}\right)\right)^{-a_3} , \tag{19}$$

where $a_1 = 3.476$, $a_2 = 0.707$ and $a_3 = -2.46$. This correlation is appropriated for the fully-rough regime ($h_{sg}^+ > 90$) and the corresponding friction resistance coefficient for a plate of length L is given by

$$C_F = \left(2.635 + 0.618 \ln\left(\frac{L}{h_{sg}}\right)\right)^{-2.5} . \tag{20}$$

Roughness also affects the near-wall mean velocity profile, which in the log-law region for a fully-rough regime is given by (Cebeci and Bradshaw, 1977):

$$\frac{V_x}{u_\tau} = \frac{1}{\kappa}\ln\left(\frac{y}{h_{sg}}\right) + B_k , \tag{21}$$

where $\kappa = 0.41$ and $B_k = 8.5$. According to Cebeci and Bradshaw (1977), in the intermediate regime[2] we have

$$\frac{V_x}{u_\tau} = \frac{1}{\kappa}\ln\left(\frac{y}{h_{sg}}\right) + B(h_{sg}^+) , \tag{22}$$

where

$$B = (1-\alpha)C + \alpha B_k + (1-\alpha)\frac{1}{\kappa}\ln\left(h_{sg}^+\right) , \tag{23}$$

$C = 5$ and

$$\alpha = \begin{cases} \sin\left[\frac{\pi}{2}\frac{\ln\left(h_{sg}^+/2.25\right)}{\ln(90./2.25)}\right] & \Leftarrow \quad 2.25 \le h_{sg}^+ \le 90. \\ 1. & \Leftarrow \quad 90 < h_{sg}^+ \end{cases} . \tag{24}$$

[2]Naturally, when h_{sg} is used for the reference length the equation does not apply to the hydraulically smooth regime.

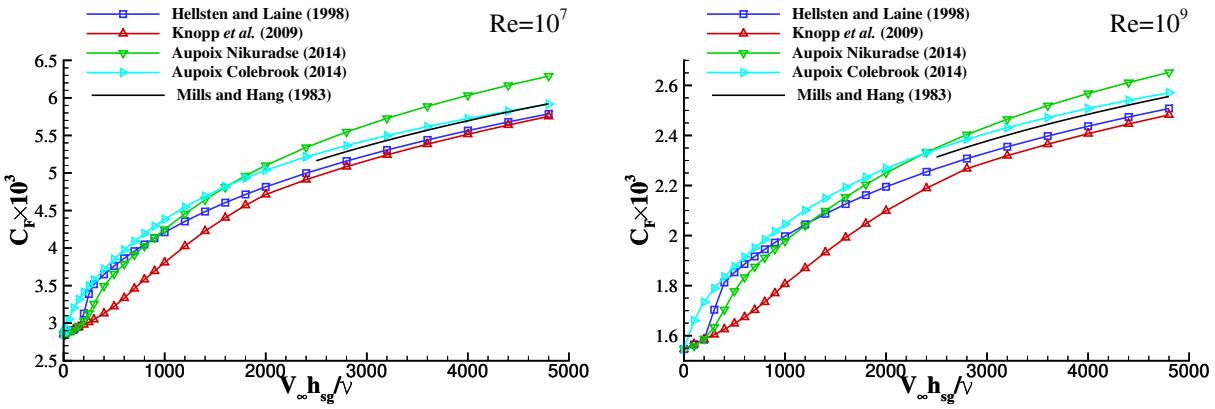

Figure 6. Friction resistance coefficient C_F of a flat plate as a function of the Reynolds number based on the sand-grain rougness height h_{sg}. Flow at $Re = 10^7$ and $Re = 10^9$.

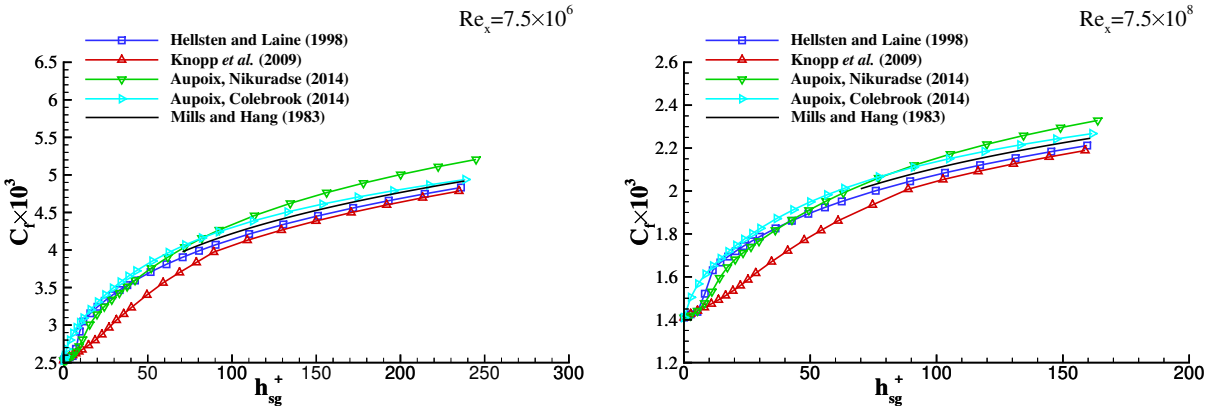

Figure 7. Skin friction coefficient C_f of a flat plate as a function of the sand-grain rougness height in wall coordinates h_{sg}^+. Locations at $x = 0.75L$ for the flows at $Re = 10^7$ and $Re = 10^9$.

4.1.2 Friction resistance coefficient, C_F

Figure 6 presents the friction resistance coefficient C_F obtained with the four approaches described in section 2.1 for the flat plate flow at Reynolds numbers of $Re = 10^7$ and $Re = 10^9$. The plots also include the results obtained from equation (20). The main trends observed in the data are similar for the two Reynolds numbers.

- The HL1998 and AN2014 exhibit the two expected inflexion points in similar locations, whereas the K2009 exhibits a wider intermediate range with a lower friction value than the other approaches. On the other hand, the AC2014 does not exhibit inflexion points;
- The AN2014 leads to the largest friction values for the fully-rough regime and the K2009 to the lowest;
- The slope of the C_F line in the fully-regime for HL1998, K2009 and AC2014 is similar to that obtained from the Mills and Hang (1983) correlation. Nonetheless, the best quantitative agreement with the data of equation (20) is exhibited by the AC2014 simulations.

All these observations are in agreement with the conclusions of Aupoix (2014).

4.1.3 Skin friction coefficient, C_f

Naturally, the results presented in the previous section are a consequence of the skin friction coefficient C_f obtained along the surface of the plate. Figure 7 illustrates the values of C_f obtained at $x = 0.75L$

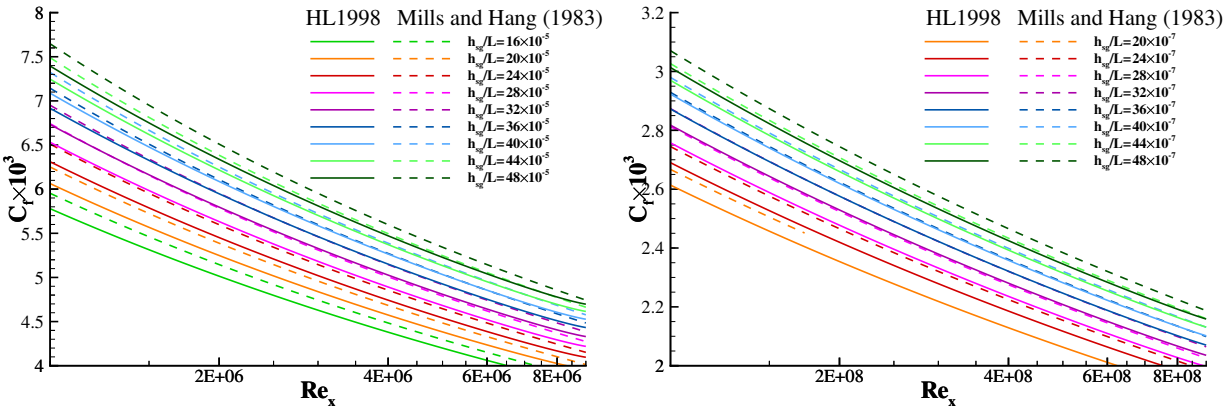

Figure 8. Skin friction coefficient C_f along the plate for sand-grain roughness heights h_{sg} in the fully-rough regime. Comparison of the results obtained with the Hellsten and Laine (1998) approach and the Mills and Hang (1983) correlation. Flows at $Re = 10^7$ and $Re = 10^9$.

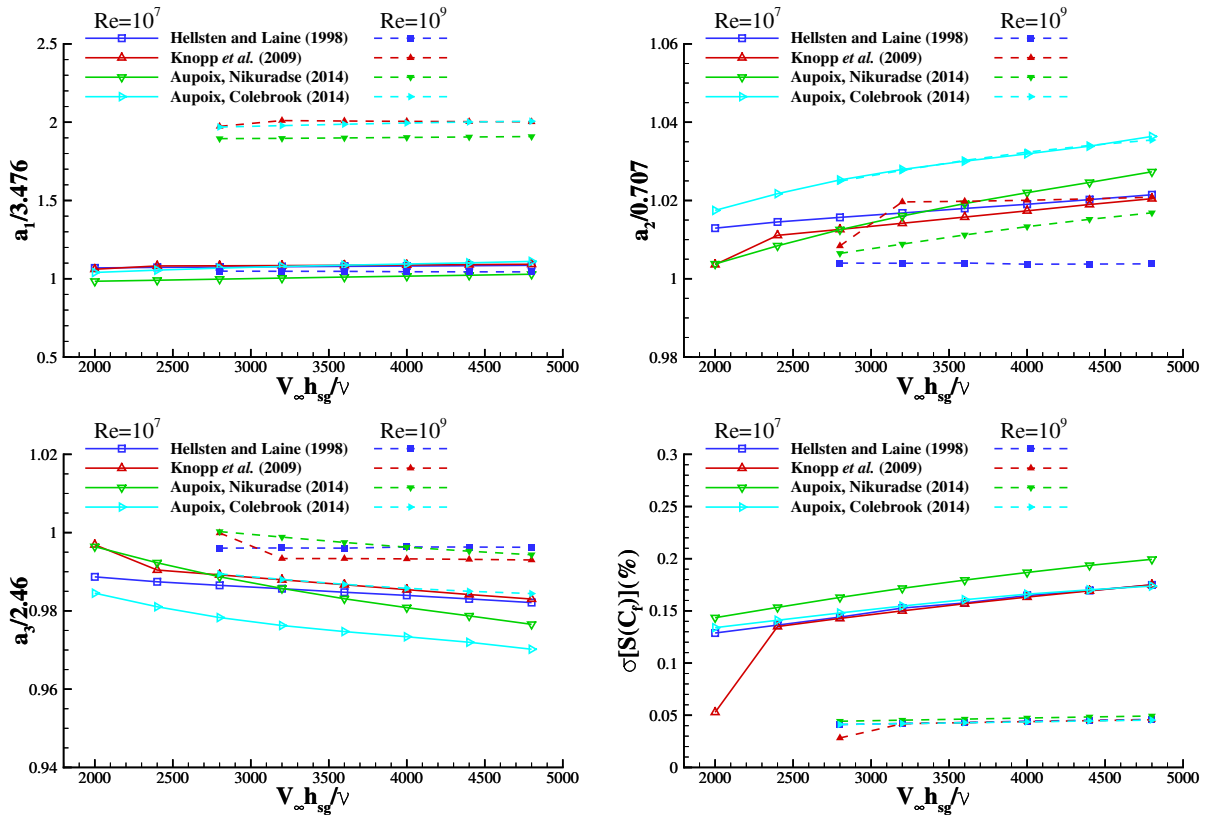

Figure 9. Constants of the fits performed to the skin friction coefficient C_f using the expression of the Mills and Hang (1983) correlation. $\sigma[S(C_f)](\%)$ is the standard deviation of the fits in percentage of the mean C_f value. Flows at $Re = 10^7$ and $Re = 10^9$.

as a function of h_{sg}^+ for the flows at $Re = 10^7$ and $Re = 10^9$. The results obtained from equation (19) proposed by Mills and Hang (1983) are also plotted in figure 7.

As expected, the trends observed in the data are similar to those discussed above for C_F. Nonetheless, it is possible to confirm that K2009 reaches the fully-rough regime for values of h_{sg}^+ larger than those exhibited by HL1998 and AN2014 and that AC2014 is only appropriate for the fully-rough regime, because the results plotted in figure 7 do not exhibit the two inflexion points at the limits of the intermediate regime. The data also confirm that the slope obtained with the AN2014 approach is larger than all the others including the reference solution, which is in agreement with Aupoix (2014). The skin friction distributions obtained with the Hellsten and Laine (1998) approach for the values of

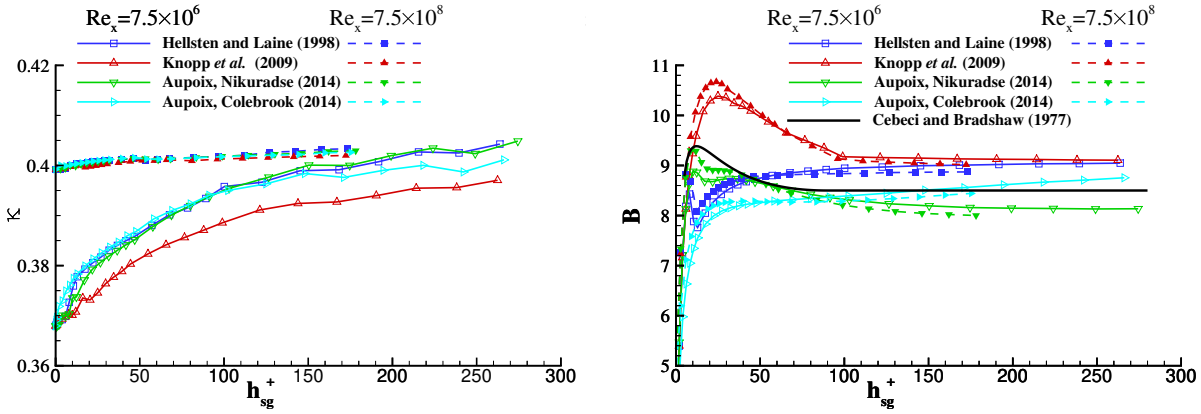

Figure 10. Constants of the mean velocity profile in the log-law region, κ and B, as a function sand-grain roughness height in wall coordinates h_{sg}^{+}. Locations at $x = 0.75L$ for the flows at $Re = 10^7$ and $Re = 10^9$.

h_{sg} in the fully-rough regime are plotted in figure 8 together with the data calculated from the Mills and Hang (1983) correlation. Although there is a shift in the value of C_f between the two approaches, the slope obtained of the C_f distributions obtained with the HL1998 option is very similar to that exhibited by the Mills and Hang (1983) correlation for both Reynolds numbers.
The C_f distributions with $h_{sg}^{+} > 90$ were fitted to equation (19) in the least-squares sense. The ratios between the fitted a_1, a_2 and a_3 and the values of the Mills and Hang (1983) correlation are presented in figure 9. The figure also presents the standard deviation of the fits in percentage of the average C_f value from each fit, $\sigma[S(C_f)](\%)$. The results show that the HL1998 leads to the best overall comparison with the Mills and Hang (1983) correlation, especially for the a_2 constant.

4.1.4 Log-law region of the mean velocity profiles

The final check of the flat plate simulations is performed for the mean velocity profiles in the log-law region. Figure 10 presents the values of κ and B obtained for the mean velocity profiles at $x = 0.75L$ of the simulations performed for $Re = 10^7$ and $Re = 10^9$. As expected (Eça and Hoekstra, 2010), for hydraulically smooth surfaces, the value of κ is smaller than $\kappa = 0.41$ for the lowest Reynolds number and it approaches the expected value with the increase of the Reynolds number. With the increase of h_{sg}^{+}, the value of κ approaches the expected value for the four techniques tested. Nonetheless, the K2009 leads to the smallest values of κ for the lowest Reynolds number plotted in figure 10.
The change of B with h_{sg}^{+} observed in the right plot of figure 10 confirms that the K2009 leads to the highest values of h_{sg}^{+} to reach the fully-rough regime. In the intermediate regime, the best agreement with the Cebeci and Smith (1977) interpolation line is obtained for the AN2014, whereas the AC2014 produces the best agreement in the fully-rough regime. However, the approach that seems to perform best in the intermediate and fully-rough regimes is the HL1998 technique. Therefore, in the remaining of this study we will restrict ourselves to the results obtained with this approach.

4.2 Dimensionless Representation of Roughness Effects on the Resistance Coefficients

Empirical correlations to estimate roughness effects on the friction resistance coefficient of ships tipically determine ΔC_F, which is the difference to the C_F value for hydraulically smooth surfaces. Three examples of these correlations are presented by the ITTC (2008):

- Bowden and Davison (1974)

$$\Delta C_F \times 10^3 = 105 \left(\frac{\mathrm{AHR}}{L_{PP}} \right)^{1/3} - 0.64 \,. \tag{25}$$

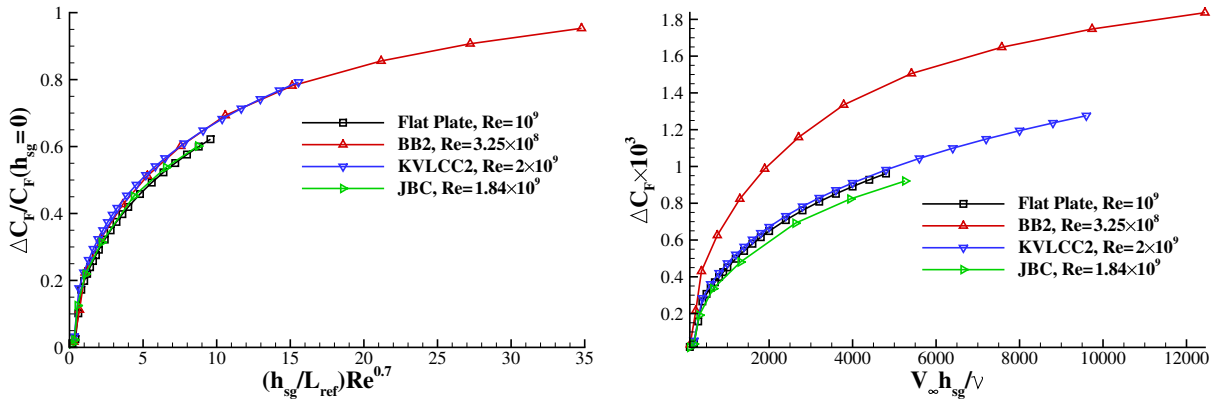

Figure 11. Increase of the friction resistance C_F with the sand-grain roughness height for the four geometries tested. Left plot includes the present proposal and the right plot the traditional representation.

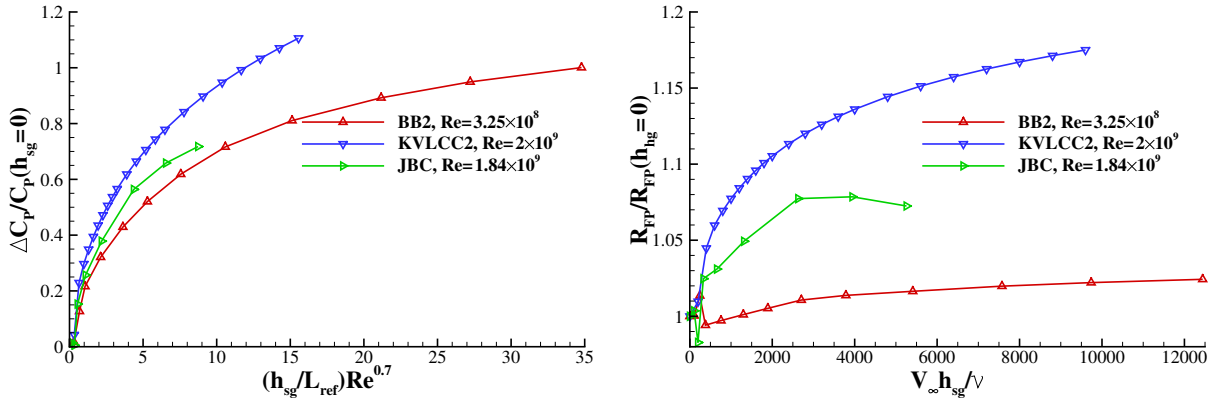

Figure 12. Increase of the pressure resistance C_P with the sand-grain roughness height in dimensionless quantities (left plot) and ratio between pressure and friction resistance coefficients $R_{FP} = C_P/C_F$ (right plot) for the three geometries tested.

- Townsin *et al.* (1984)

$$\Delta C_F \times 10^3 = 44 \left[\left(\frac{\mathrm{AHR}}{L_{PP}} \right)^{1/3} - 10 Re^{-1/3} \right] + 0.125 \, . \tag{26}$$

- Himeno

$$\Delta C_F \times 10^3 = 18 \left(\frac{\mathrm{AHR}}{L_{PP}} \right) Re^{0.75} \, . \tag{27}$$

Assuming that there is a coefficient that relates AHR to h_{sg}, ΔC_F must change with the Reynolds number, because C_F of a smooth surface decays with the Reynolds number and C_F of a fully-rough surface becomes independent of the Reynolds number. Therefore, with the purpose of obtaining a single line that quantifies roughness effects, it is more logical to use $\Delta C_F/C_F(h_{sg} = 0)$, where $C_F(h_{sg} = 0)$ is the friction resistance coefficient for an hydraulically smooth surface. Taking into account C_F should depend on h_{sg}^+, we have determined $\Delta C_F/C_F(h_{sg} = 0)$ as a function[3] of $(h_{sg}/L_{PP})Re^{0.7}$ for all the geometries tested in this study.

Figure 11 presents the increase of the friction resistance as a function the sand-grain roughness height for the four geometries tested using the present proposal and the standard representation. Although the overlap between the four geometries tested is not perfect, the choice of dimensionless quantities proposed in this study leads to very similar results for the four cases. Furthermore, there is an almost perfect match between the BB2 and KVLCC2 results that were obtained at Reynolds numbers that

[3]The exponent 0.7 was selected to obtain the best agreement between the results of the four geometries tested.

Table 2. Ratio between AHR and h_{sg} and standard deviation σ_α of the least-squares fits of the friction resistance coefficient C_F to the Bowden and Davison (1974) and Townsin *et al.* (1984) correlations using AHR $= \alpha h_{sg}$ for the four tested geometries.

Test Case	Re	Bowden and Davison (1974)		Townsin *et al.* (1984)	
		α	σ_α	α	σ_α
Flat Plate	10^9	0.78	0.17	5.2	0.004
BB2 submarine	3.25×10^8	0.44	0.67	5.03	0.14
KCLCC2 tanker	2×10^9	1.35	0.21	8.4	0.006
JBC ship	1.84×10^9	1.31	0.44	6.36	0.01

differ one order of magnitude. In the traditional representation of ΔC_F there is a clear difference between the BB2 and KVLCC2 results.

If the ratio between pressure and friction resistance coefficients $R_{FP} = C_P/C_F$ is independent of h_{sg}, the results presented in figure 11 for C_F could be replicated for C_P. However, as illustrated in figure 12, there is a signficant influence of h_{sg} on R_{FP} for the three practical geometries tested. Therefore, the lines presented in the left plot of figure 12 exhibit much larger differences than those obtained for C_F.

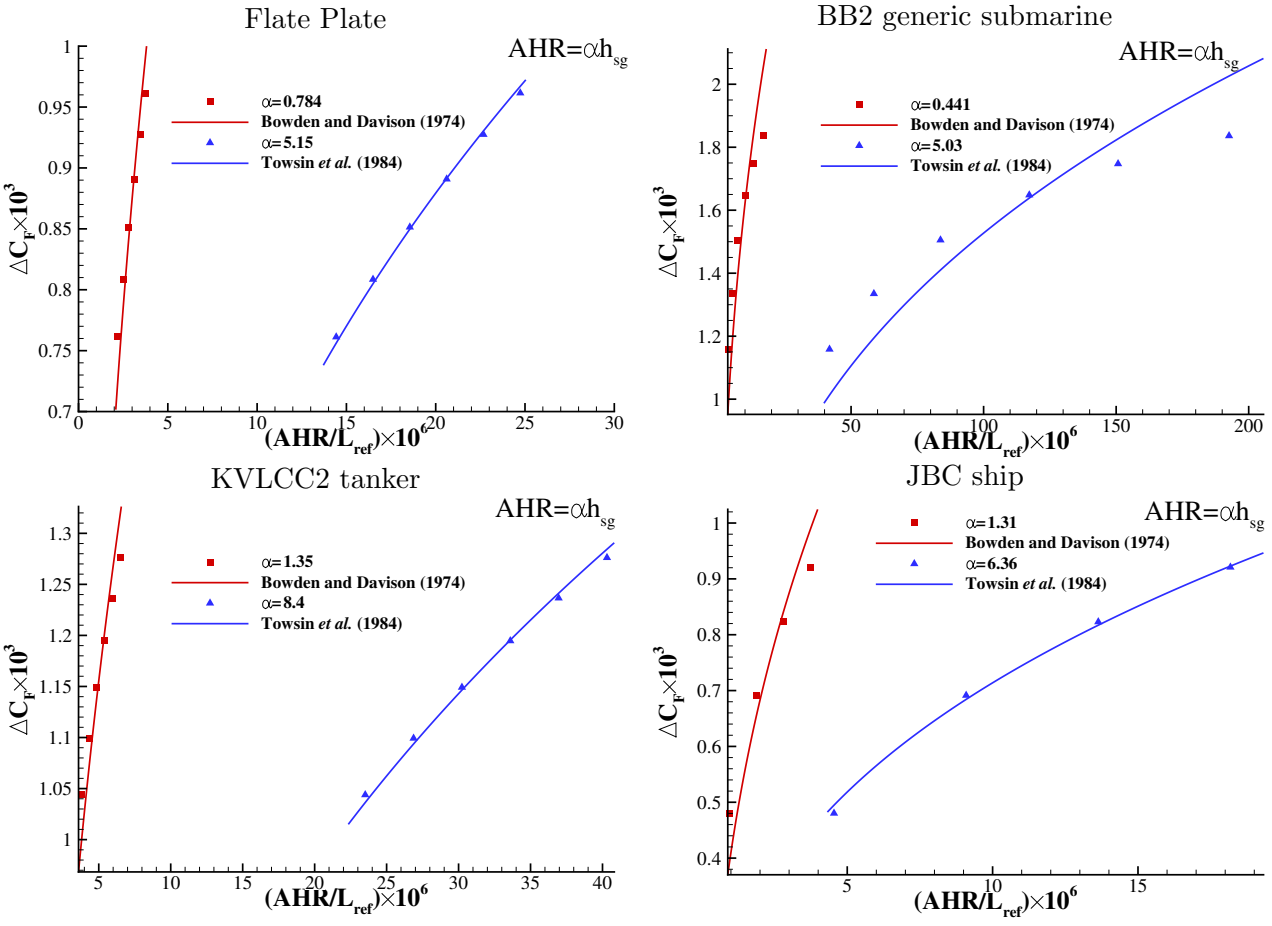

Figure 13. Least-squares fits of the friction resistance coefficient C_F to the Bowden and Davison (1974) and Townsin *et al.* (1984) correlations using AHR $= \alpha h_{sg}$ for the four tested geometries.

4.3 Relation between Average Hull Roughness and Sand-Grain Roughness Height

The Bowden and Davison (1974) and Townsin *et al.* (1984) correlations[4], equations (25) and (26), were fitted to the C_F data in the fully-rough regime using AHR $= \alpha h_{sg}$ in the least-squares sense. The goal is to determine the ratio α between AHR and h_{sg} and the agreement between the correlations and the simulations.
Figure 13 and table 2 present the least-squares fits to the C_F data, the values of α and the standard deviation of the fits σ_α for the four selected geometries. The data show the following trends:

- The simulations are in better agreement with the Townsin *et al.* (1984) correlation than with the Bowden and Davison (1974) correlation;
- The poorest agreement between the simulations and the Townsin *et al.* (1984) correlation is obtained for the BB2 submarine that exhibits the lowest Reynolds number;
- The values of α obtained from the Bowden and Davison (1974) correlation do not seem reliable, whereas the α derived from the Townsin *et al.* (1984) correlation is close to the factor of 5 suggested by Schultz (2007) for antifouling coating. However, the value of α depends on the selected geometry.

With the exception of the BB2 submarine, the present results suggest that a value of α independent of the roughness height produces an excellent agreement between the simulations and the Towsin *et al.* correlation. The two ships should be also simulated at a Reynolds number of the order of 10^8 to check if the agreement between simulations and correlation depends on the Reynolds number.

5 CONCLUSIONS

The present paper presents a study on roughness effects in the flows around four geometries: a flat plate; the BB2 generic submarine; the KVLCC2 tanker and the JBC ship. Simulations are performed with RANS solvers using the SST $k-\omega$ two-equation eddy-viscosity model and four alternative wall boundary conditions for k and ω that model roughness effects using the equivalent sand-grain roughness height h_{sg}.
A preliminary study is performed for the flat plate at Reynolds numbers of 10^7 and 10^9 to compare the four roughness models selected. The results are in agreement with the observations of Aupoix (2014), with the Knopp *et al.* (2009) proposal leading to the lowest values of the increase of C_F and to the widest range of values for the intermediate regime. The approach based on the Colebrook correlation does not exhibit the inflexion points that characterize the limits of the intermediate regime and the approach based on the Nikuradse correlation leads to the largest slope of the C_F increase in the fully-rough regime. Globaly, the Hellsten and Laine (1998) proposal exhibits the most consistent results and so it was selected to perform the study for the three practical geometries.
The simulations performed for the practical geometries focused on two different aspects of roughness modeling: the choice of dimensionless quantities to represent the increase of friction resistance and the use of empirical correlations based on the average roughness height (AHR) to assess the conversion between AHR and h_{sg}. The results of the simulations lead to the following conclusions:

- It is possible to select dimensionless quantities that make the effect of sand-grain roughness on the friction resistance of the four selected geometries collapse (almost) to a single line. The proposed representation uses $(h_{sg}/L_{ref})Re^{0.7}$ as the independent variable and ΔC_F divided by C_F for an hydraulically smooth wall as the dependent variable.
- In the present test cases, the ratio between the pressure and friction resistance depends on the sand-grain roughness size. Therefore, the proposal that collapses the friction resistance results does not lead to the same result for the pressure resistance.

[4]We have also tested the Himeno correlation, but the values of α obtained do not make sense.

- The simulations are in better agreement with the Townsin *et al.* correlation than with the Bowden and Davison correlation. Ratio between AHR and h_{sg} obtained from the Townsin *et al.* depends on the selected geometry and is close to the value suggested by Schultz for antifouling coating.

In the present study, a formal numerical uncertainty estimation was only performed for the flat plate at a Reynolds number of 10^7. Therefore, the next step of this study is to confirm that the trends found in the results are not polluted by numerical uncertainties.

ACKNOWLEDGEMENTS

This research is partly funded by the Dutch Ministry of Economic Affairs.

REFERENCES

Andersson J., Oliveira D.R., Yeginbayevab I., Leer-Andersen M. and Bensow R.E. (2020), Review and comparison of methods to model ship hull roughness. Applied Ocean Research. Vol. 99.

Aupoix B. (2014), Wall Roughness Modelling with k-w STT Model. 10^{th} International ERCOFTAC Symposium on Engineering Turbulence Modelling and Measurements, Marbella, Spain.

Bowden, B. S., and Davison, N. J. (1974), Resistance Increments Due to Hull Roughness Associated With Form Factor Extrapolation Methods, National Physical Laboratory (NP) Ship Technical Manual 3800.

Carrica P.M, Kerkvliet M., Quadvlieg F. H. H. A., Pontarelli M. and Martin J. E. (2016), Simulations and Experiments of a Maneuvering Generic Submarine and Prognosis for Simulation of Near Surface Operation, 31^{st} Symposium on Naval Hydrodynamics, Montery, California, U.S.A.

Cebeci T., Bradshaw P. (1977), Momentum Transfer in Boundary Layers, Hemisphere Publishing Corporation, New York.

Churchill S.W. (1993), Theoretically based expressions in closed form for the local and mean coefficients of skin friction in fully turbulent flow along smooth and rough plates. International Journal of Heat and Fluid Flow, 14(3), pp. 231 239.

Eça L, Hoekstra M. (2004), On the Grid Sensitivity of the Wall Boundary Condition of the $k-\omega$ model, Journal of Fluids Engineering, Vol. 126, N^o 6, pp. 900-910.

Eça L., Hoekstra M. (2008), The Numerical Friction Line, Journal of Marine Science and Technology, Vol. 13, Number 4, pp-328-345.

Eça L. and Hoekstra M. (2010), Nearwall profiles of mean flow and turbulence quantities predicted by eddyviscosity turbulence models. Int. J. Numer. Meth. Fluids, 63 pp: 953-988. https://doi.org/10.1002/fld.2115.

Eça L., Hoekstra M. and Raven H.C. (2010), Quantifying roughness effects by ship viscous flow calculations 28th Symposium on Naval Hydrodynamics, Pasadena, California, USA.

Eça L. and Hoekstra M. (2011), Numerical aspects of including wall roughness effects in the SST $k-\omega$ eddy-viscosity turbulence model, Computers & Fluids, Vol. 40, Issue 1, Pages 299-314.

Eça L., Pereira F.S., Vaz G. (2018), Viscous flow simulations at high Reynolds numbers without wall functions: Is $y^+ \simeq 1$ enough for the near-wall cells?, Computers & Fluids, Vol.170, pp.157-175.

Hellsten A., Laine S. (1998), Extension of the $k-\omega$ shear-stress transport turbulence model for rough-wall flows, AIAA Journal, Vol. 36, pp. 1728-1729.

Hino T., Stern F., Larsson L. Visonneau M., Hirata N., and Kim J. (Eds.), (2016), Numerical Ship Hydrodynamics, an assessment of the Tokyo 2015 Workshop, Tokyo, Japan.

Hoekstra M. and Eça L. (1998), PARNASSOS: An Efficient Method for Ship Stern Flow Calculation, Third Osaka Colloquium on Advanced CFD Applications to Ship Flow and Hull Form Design, Osaka, Japan.

ITTC (2008), The Resistance Committee Final Report and Recommendations to the 25$^{\text{th}}$ ITTC, Fukuoka, Japan.

Knopp T., Eisfeld B., Calvo J.B. (2009), A new extension for $k?\omega$ turbulence models to account for wall roughness, International Journal of Heat and Fluid Flow, Vol. 30, pp. 54-65.

Larsson L., F. Stern F. and Bertram V. (Eds.) (2002), Gothenburg 2000 - A Workshop on Numerical Ship Hydrodynamics, Chalmers University of Technology, Gothenburg, Sweden.

Larsson L., Stern F. and Visonneau M. (Eds.) (2010), Gothenburg 2010 - A Workshop on Numerical Ship Hydrodynamics, Chalmers University of Technology, Gothenburg, Sweden.

Menter F.R. (1994), Two-Equation Eddy-Viscosity Turbulence Models for Engineering Applications, AIAA Journal, Vol. 32, No. 8, pp. 1598–1605.

Mills A. F. and Hang X. (1983), On the skin friction coefficient for a fully rough flat plate, Journal Fluids Engineering, Vol. 105(3):364?365.

Pereira F.S., Eça L., Vaz G. and Kerkvliet M. (2019), Application of second-moment closure to statistically steady flows of practical interest, Ocean Engineering, Volume 189,
DOI: 10.1016/j.oceaneng.2019.106372

Pimenta M. M., Moffat R. J. and Kays W. M. (1975), The Turbulent Boundary Layer: An Experimental Study of the Transport of Momentum and Heat with the Effect of Roughness, Department of Mechanical Engineering, Stanford University.

ReFRESCO, (2021), `https://www.marin.nl/facilities-and-tools/software/refresco`

Schultz, M.P. (2007), Effects of coating roughness and biofouling on ship resistance and powering. Biofouling, 23(5-6):331-41. DOI: 10.1080/08927010701461974.

Toxopeus S.L., Bettle M.C., Uroić T., Guilmineau E., Bordier L., Olbert G., Bensow R.E., Petterson K., Dikbaş E., Feldman J. and Pattenden R. (2019), NATO AVT-301 Collaborative Exercise: CFD Predictions for BB2 Generic Submarine, Phase 0 – Pre-Test Computations, NATO STO AVT-307 Research Symposium on Separated Flow: Prediction, Measurement and Assessment for Air and Sea Vehicles, Trondheim, Norway.

Townsin, R.L., Medhurst, J.S., Hamlin, N.A. and Sedat, B.S. (1984), Progress in calculating the resistance of ships with homogeneous or distributed roughness, NECIES Centenary Conference in Marine Propulsion, Newcastle upon Tyne, United Kingdom.

Wilcox D.C. (1988), Reassessment of the scale- determining equation for advanced turbulence models, AIAA Journal, Vol. 26, pp. 1299-1310.

Wilcox D.C. (2006), Turbulence Modeling for CFD - DCW Industries, 3$^{\text{rd}}$ Edition.

Yeginbayeva, I.A. and Atlar, M. (2018), An experimental investigation into the surface and hydrodynamic characteristics of marine coatings with mimicked hull roughness ranges, Biofouling, 34:9, 1001-1019, DOI: 10.1080/08927014.2018.1529760.